

# Calculating thermal conductivity in a transient conduction regime: theory and implementation

Claudio Melis, Riccardo Dettori, Simon Vandermeulen, and Luciano Colombo<sup>a</sup>

Dipartimento di Fisica, Università di Cagliari Cittadella Universitaria, 09042 Monserrato (Ca), Italy

Received 21 February 2014 / Received in final form 12 March 2014

Published online (Inserted Later) – © EDP Sciences, Società Italiana di Fisica, Springer-Verlag 2014

**Abstract.** We present a molecular dynamics method addressed to the calculation of the lattice thermal conductivity during the transient regime of approach to equilibrium from an initial condition of nonuniform temperature profile. We thoroughly assess the basics, the robustness, and the accuracy of the method, in particular by showing that its results are basically independent of most of the arbitrary simulation parameters. In addition, the method here presented is computationally light, thus paving the way for the investigation of large systems. This feature is fully exploited to investigate the thermal transport properties of disordered and nanostructured silicon samples, providing a clear atomistic picture on the ability of grain boundaries and lattice disorder to affect thermal conductivity by improved scattering of vibrational modes with long mean free path.

## 1 Introduction

While a basic understanding of heat transport at the macroscopic scale has already been achieved [1,2], many important issues concerning its atomic-scale details are still a matter of intense research. For instance, a full understanding of the heat transport phenomena at the nanoscale is of crucial importance to improve both performance and function of novel thermoelectric as well as heat sink materials [3–8]. For this reason, atomistic simulations (like, e.g., molecular dynamics simulations, Boltzmann transport equation, and Green’s function approaches) represent a valuable tool for addressing the atomistic details of thermal transport: as a matter of fact, they are extensively used to address various aspects of thermal transport phenomena in complex materials [8–11].

In this work, we focus on molecular dynamics (MD), where nanoscale structural features, as well as phonon-phonon interactions, are in principle described exactly. In particular, we critically address the approach to equilibrium MD method (hereafter referred to as AEMD) which has been recently introduced [12] and successfully applied to predict thermal conductivity in nanoscale semiconductor systems [13,14].

Two different techniques are mainly used to model the heat transport by MD, namely: equilibrium (EMD) and nonequilibrium (NEMD) molecular dynamics. EMD calculates the thermal conductivity  $\kappa$  at temperature  $T$  along a given  $z$  direction using the equilibrium fluctuations of the heat current vector  $j$  through the current-current

autocorrelation function [15]

$$\kappa = \frac{1}{k_B T^2 V} \int_0^{+\infty} \langle j_z(t) j_z(0) \rangle dt \quad (1)$$

where  $k_B$  is the Boltzmann constant,  $V$  is the system volume, and  $\langle \dots \rangle$  indicates the ensemble average.

NEMD [8,16,17] instead, calculates  $\kappa$  in analogy to the experimental measurement, i.e. by means of the Fourier law

$$j_z = -\kappa \frac{\partial T}{\partial z} \quad (2)$$

where the external perturbation  $\partial T/\partial z$  and the system response  $j_z$  are separately computed, eventually getting the thermal conductivity as the response-to-perturbation ratio  $\kappa = -\langle j_z \rangle / \partial T / \partial z$ . Usually the NEMD method is implemented on the approach proposed by Müller-Plathe [8,16], where the periodically-repeated simulation box is divided into  $N_s$  slabs. Slab 0 is defined as the hot slab and slab  $N_s/2$  is the cold slab. The heat flux is generated by exchanging the kinetic energy between the hottest atom in the cold slab and the coldest atom in the hot slab in order to decrease the temperature in the cold slab and increase it in the hot one. After a suitable number of exchanges a nonequilibrium steady state is eventually reached and both  $\langle j_z \rangle$  and  $\partial T/\partial z$  are easily computed. Alternatively, a thermal gradient can be established by thermostating the two opposite terminal layers of a finite-thickness slab at different temperatures, while its inner part is evolved microcanonically. After a long enough simulation, a steady state thermal gradient is so generated and the corresponding  $\langle j_z \rangle$  calculated.

<sup>a</sup> e-mail: luciano.colombo@dsf.unica.it

Even though both EMD and NEMD methods are largely used to describe thermal transport phenomena in a variety of different systems, they suffer from several drawbacks which often limit their applications to atomistic models large enough to properly describe a given complex nanostructure. As far as concerns the EMD methods, their main limitation is the very long time needed to converge the current-current autocorrelation function [8]. It has been shown recently [9] that as many as  $\mathcal{O}(10^6)$  atoms and several hundred thousands MD time-steps are indeed necessary to provide a fully converged value of lattice thermal conductivity in a system such as bulk crystalline silicon. In turn, NEMD methods are mainly limited by the very long simulation time needed to establish a steady state condition, once that a given temperature gradient or heat current is imposed.

In this work we rather use AEMD in which the simulation is performed in a transient thermal conduction regime. The system is initially set out of equilibrium by imposing a step-like temperature difference  $\Delta T$  between the left- and right-half of the simulation cell. Then, the time evolution of  $\Delta T(t)$  is monitored during a microcanonical (NVE) MD run until the system reaches the equilibrium, corresponding to  $\Delta T = 0$ . It is shown below that  $\kappa$  can be easily estimated by fitting the  $\Delta T(t)$  with a suitable solution of the heat equation. The typical simulation time needed to reach the equilibrium is comparatively much shorter than in EMD or NEMD calculations, thus paving the way for simulations with unprecedented size.

The primary goal of the present work is methodological, namely: to assess the accuracy and performances of the AEMD method against several simulation parameters. In particular, we study the dependence of the estimated thermal conductivity  $\kappa$  on each single method-specific feature and gauge AEMD reliability on several benchmark systems of current interest, i.e. crystalline, amorphous and nanocrystalline silicon.

## 2 Approach to equilibrium molecular dynamics

Heat transport is described by means of the heat equation [9]

$$\frac{\partial T}{\partial t} = \bar{\kappa} \frac{\partial^2 T}{\partial z^2} \quad (3)$$

where  $\bar{\kappa} = \kappa/\rho c_v$  is the thermal diffusivity of the system with density  $\rho$  and specific heat  $c_v$ . We assume that  $\kappa$ ,  $\rho$  and  $c_v$  do not depend neither on  $t$  nor on  $z$  over the period of time corresponding to the typical duration of the simulation.

Equation (3) can be solved by separating the variables

$$T(z, t) = H(z)T(t) \quad (4)$$

leading, after some algebra, to

$$T(z, t) = \sum_{n=1}^{\infty} [A_n \cos(\alpha_n z) + B_n \sin(\alpha_n z)] e^{-\alpha_n^2 \bar{\kappa} t} \quad (5)$$

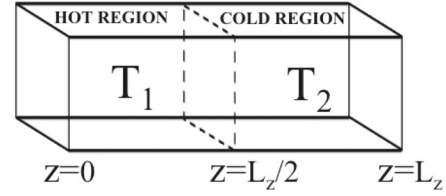


**Fig. 1.** Sketch of the simulation cell used in the AEMD simulations, with periodic boundary conditions along any direction. The hot ( $0 < z < L_z/2$ ) and cold ( $L_z/2 < z < L_z$ ) regions are initially set at temperature  $T_1$  and  $T_2$ , respectively, with  $T_1 > T_2$ .

where  $\alpha_n = 2\pi n/L_z$ , while  $A_n$  and  $B_n$  depend only on the initial condition  $T(z, 0) = H(z)$  through the following expressions

$$A_n = \frac{1}{L_z} \int_0^{L_z} \cos(\alpha_n z) H(z) dz \quad (6)$$

$$B_n = \frac{1}{L_z} \int_0^{L_z} \sin(\alpha_n z) H(z) dz. \quad (7)$$

By considering a system defined in an interval with  $0 \leq z \leq L_z$  (see Fig. 1), three kinds of boundary conditions (BCs) are commonly encountered in heat transfer problems, namely: (i) Dirichlet BCs set as  $T(0, t) = 0 = T(L_z, t)$ ; (ii) von Neumann BCs set as  $\frac{\partial T}{\partial z}(0, t) = 0 = \frac{\partial T}{\partial z}(L_z, t)$ ; and (iii) periodic BCs set as  $T(0, t) = T(L_z, t)$  and  $\frac{\partial T}{\partial z}(0, t) = \frac{\partial T}{\partial z}(L_z, t)$ . Since we aim at applying this formalism to MD simulations, the natural choice is selecting periodic BCs. In particular, we set the following step-like temperature profile

$$H(z) = \begin{cases} T_1 & \text{for } 0 < z < L_z/2 \\ T_2 & \text{for } L_z/2 < z < L_z \end{cases}$$

which is also shown in Figure 1.

In this case the general solution of equation (3) is:

$$T(z, t) = A_0 + \sum_{n=1}^{\infty} B_n \sin(\alpha_n z) e^{-\alpha_n^2 \bar{\kappa} t} \quad (8)$$

where

$$A_0 = \frac{1}{L_z} \int_0^{L_z} H(z) dz = \frac{T_1 + T_2}{2} \quad (9)$$

$$B_n = \frac{1}{L_z} \int_0^{L_z} \sin(\alpha_n z) H(z) dz = \frac{T_1 - T_2}{\alpha_n L_z} [\cos(\alpha_n L_z) - 1] \quad (10)$$

while under these conditions for  $n \neq 0$  we get

$$A_n = \frac{1}{L_z} \int_0^{L_z} \cos(\alpha_n z) H(z) dz = 0. \quad (11)$$

By now ageing the system in a microcanonical MD simulation, the initial step-like temperature profile is progressively smoothed by thermal conduction and, therefore,

the average temperatures  $\langle T_1 \rangle$  and  $\langle T_2 \rangle$  in the two semi-cells

$$\langle T_1 \rangle = \frac{1}{L_z} \int_0^{L_z/2} T(z, t) dz \quad (12)$$

and

$$\langle T_2 \rangle = \frac{1}{L_z} \int_{L_z/2}^{L_z} T(z, t) dz \quad (13)$$

vary in time toward approaching a uniform temperature (i.e. equilibrium) configuration. During such a transient regime we can define the time-dependent difference in average temperatures  $\Delta T(t) = \langle T_1 \rangle - \langle T_2 \rangle$  which, through equation (8), is easily shown to be:

$$\Delta T(t) = \langle T_1 \rangle - \langle T_2 \rangle = \sum_{n=1}^{\infty} C_n e^{-\alpha_n^2 \bar{\kappa} t} \quad (14)$$

where

$$C_n = 8(T_1 - T_2) \frac{[\cos(\alpha_n L_z/2) - 1]^2}{\alpha_n^2 L_z^2}. \quad (15)$$

Equation (14) is the key equation of the AEMD method, which actually proceeds through three simple steps:

- an initial periodic step-like temperature profile is generated within the simulation cell;
- the system is then aged by a microcanonical run, during which the  $\Delta T(t)$  function is computed;
- after collecting such a function during a long enough simulation (see below),  $\Delta T(t)$  is fitted by equation (14) and the thermal diffusivity is straightforwardly calculated.

The corresponding thermal conductivity is eventually evaluated as  $\kappa = \bar{\kappa} \rho c_v$ , where quantum corrections below the Debye temperature ( $\Theta_D$ ) should be duly considered for the specific heat. In detail, we have:

$$\kappa = \bar{\kappa} \rho c_v = \frac{\bar{\kappa} \mathcal{C}_v}{V} \quad (16)$$

where  $\mathcal{C}_v$  is the heat capacity for  $T > \Theta_D$

$$\mathcal{C}_v = 3N K_B \quad (17)$$

and quantum corrections, taking into account the deviations from the Maxwell-Boltzmann distribution below the Debye temperature [18], are usually inserted by renormalizing  $C_v$  by a factor  $\bar{q}$  defined, in turn, as the ratio between the actual temperature and the Debye temperature. In particular, for c-Si at 600 K we get  $\bar{q} = 0.947$  and for a-Si at 300 K we get  $\bar{q} = 0.891$ .

### 3 Assessing AEMD

As a test case for assessing the AEMD accuracy and robustness we use c-Si at 600 K whose thermal conductivity

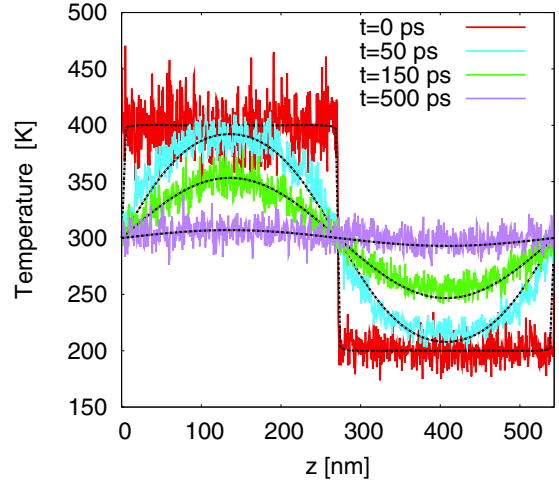


**Fig. 2.** Time evolution of the temperature profile across a c-Si sample with  $L_z = 543.2$  nm and  $S = 3.80 \times 3.80$  nm $^2$  as obtained by solving analytically equation (3) (smooth lines) and by direct MD calculation of local temperature (noisy color lines).

has been experimentally measured [19] and theoretically calculated [20,21]. All the simulations are performed at an average temperature of 600 K which is close to the Si Debye temperature of 625 K. This choice allows to minimize the quantum corrections to the heat capacity, thus allowing for a cleaner interpretation of any true AEMD feature.

#### 3.1 Computational details

All the simulations are performed using the LAMMPS [22] package and the Environment Dependent Interatomic Potential (EDIP) [23]. This potential consists of a functional form incorporating several coordination dependent functions in order to adapt the Si-Si interactions to any possible bonding configuration. For this reason, EDIP is particularly suitable for the description of non-crystalline systems such as the nano-crystalline and amorphous Si simulated here. In all simulations below the equations of motions have been integrated by the velocity-Verlet algorithm with a time step as short as  $10^{-15}$  s.

The AEMD simulation protocol requires at first the creation of a (periodic) temperature profile with a given initial step  $\Delta T(0)$ : in the present simulations this step is operated by Nosé-Hoover thermostating, paying attention to avoid any heat exchange during the thermostating period. To this aim we first (then) equilibrate the hot (cold) region at temperature  $T_1$  ( $T_2$ ) by keeping fixed all atoms in the cold (hot) region. Figure 2 shows the time evolution of a step-like temperature profile with  $\Delta T(0) = 200$  K generated across a c-Si sample with  $L_z = 543.2$  nm: while the smooth lines represent the formal solutions of equation (3), the noisy lines represent the direct MD calculation of the local temperature, during a microcanonical run. In Figure 2 the local temperature  $T(z, t)$  was calculated as an average over  $10^3$  time steps taken on a

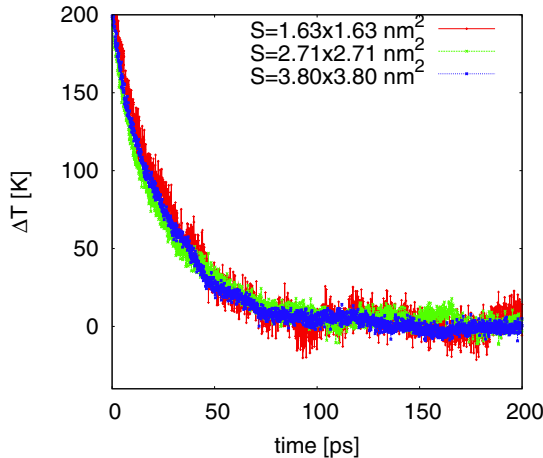


**Fig. 3.** Time evolution of  $\Delta T(t)$  during the microcanonical MD run for three samples with  $L_z = 108.61$  nm, but different cross sections  $S$ . The initial temperature difference between the hot and cold regions is  $\Delta T(0) = 200$  K.

thin slab centered at  $z$  with thickness 0.5432 nm. The simulated local temperature and the one obtained from the formal solution are in very good agreement, indicating that the use of the Fourier law is valid for these type of simulations. Furthermore, it evidences the applicability of the AEMD method at such length scales, typical of a molecular dynamics simulation.

### 3.2 $\kappa$ dependence on the sample cross section

We first explore the  $\kappa$  dependence on the cross section  $S$  by considering eight different c-Si samples with  $L_z = 108.61$  nm and  $S$  ranging from  $1.63 \times 1.63$  nm $^2$  to  $4.34 \times 4.34$  nm $^2$ . The initial temperature of the hot and cold regions is  $T_1 = 700$  K and  $T_2 = 500$  K, respectively, corresponding to  $\Delta T(0) = 200$  K. In Figure 3 we show the time evolution of  $\Delta T(t)$  during the following microcanonical MD run for just three samples for sake of clarity. We remark that, for any value of  $S$ , the system evolves towards  $\Delta T_{eq} = 0$  K value in a transient time of equal duration. Larger instantaneous oscillations of  $\Delta T(t)$  are observed for samples with smaller cross section. This is due to the fact that the average temperatures from equations (12) and (13) are calculated on a smaller number of atoms.

Figure 4 shows the calculated  $\kappa$  values for all samples with different cross section. As expected,  $\kappa$  is only marginally dependent on the sample section as compared to the  $\kappa$  dependence on the sample length (see below). For sections larger than  $2.17 \times 2.17$  nm $^2$ ,  $\kappa$  converges to a value of  $18.2 \pm 0.1$  W m $^{-1}$  K $^{-1}$ . Therefore, in all the AEMD simulations below we consider cross sections larger than  $2.17 \times 2.17$  nm $^2$  as the best choice with optimal accuracy/cost ratio.

### 3.3 $\kappa$ dependence on the initial temperature profile

In equation (3) we assumed that  $\kappa$  is not dependent on the  $z$  position. In our AEMD simulations this assumption

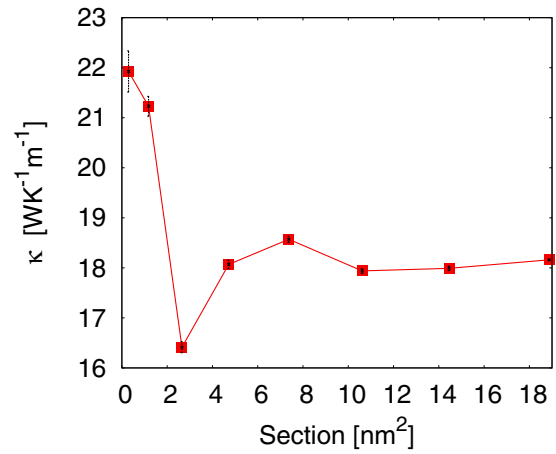


**Fig. 4.** Calculated  $\kappa$  for 8 c-Si samples with  $L_z = 108.61$  nm, but different cross sections  $S$ . The initial temperature difference between the hot and cold regions is  $\Delta T(0) = 200$  K.

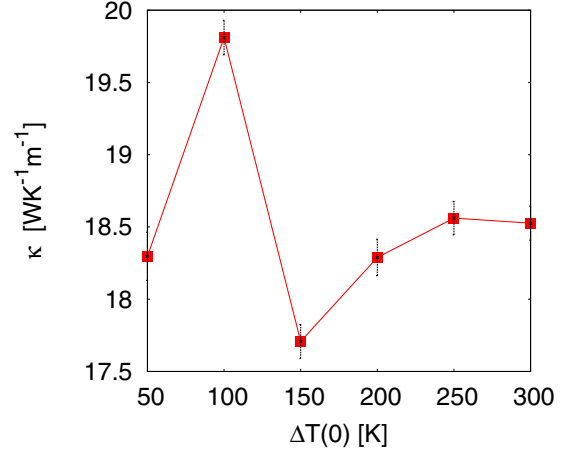


**Fig. 5.** Calculated  $\kappa$  for a c-Si sample with  $L_z = 108.61$  nm and  $S = 3.80 \times 3.80$  nm $^2$  as function of the initial temperature difference between the hot and cold regions.

is indeed not strictly satisfied since  $\kappa$  is actually a function of temperature, which is in turn a function of  $z$ . In order to assess the limitations of the present assumption we perform a series of simulations where the initial temperature difference  $\Delta T(0)$  between the hot and cold regions was set at 6 different values, namely: 50 K, 100 K, 150 K, 200 K, 250 K and 300 K. Figure 5 shows  $\kappa$  as a function of  $\Delta T(0)$  for a system with  $L_z = 108.61$  nm and cross section  $3.80 \times 3.80$  nm $^2$ . Also in this case we do not observe any meaningful dependence on  $\Delta T(0)$ . However for  $\Delta T(0)$  greater than 150 K the error significantly decreases and  $\kappa$  converges to a value of  $18.5 \pm 0.1$  W m $^{-1}$  K $^{-1}$ . Therefore, in all the AEMD simulations below we set  $\Delta T(0) = 200$  K.

Despite the reassuring results discussed above, we remark that under high temperature differences, various domains of the simulation cell are likely characterized by different thermal conductivities (especially in the case of highly conductive materials and/or very long simulation cells). Therefore, the information extracted by AEMD

**Table 1.** Calculated  $\kappa$  for a system with  $L_z = 162.91$  nm and  $S = 3.80 \times 3.80$  nm $^2$  by using a different number  $N_{exp}$  of exponentials in equation (15).

$N_{exp}$	$\kappa$ (W m $^{-1}$ K $^{-1}$ )
1	$23.2 \pm 0.3$
2	$23.3 \pm 0.2$
5	$23.4 \pm 0.2$
10	$23.4 \pm 0.2$
20	$23.4 \pm 0.2$
500	$23.4 \pm 0.2$

simulation (i.e. the value of  $\kappa$ ), should be regarded as an effective linear response to thermal gradients.

### 3.4 $\kappa$ dependence on the fitting procedure for $\Delta T(t)$

Another important issue to be addressed is the  $\kappa$  dependence on the number of exponentials  $N_{exp}$  used in equation (14) to fit  $\Delta T(t)$ . In principle an infinite number of terms should be used in order to obtain the best fit of  $\Delta T(t)$ . However, the computational cost of the fitting procedure strongly increases with the number of exponentials. For this reason our goal is to use the minimum number of exponentials providing an accurate  $\kappa$  value. The results are summarized in Table 1 where we calculate  $\kappa$  using  $N_{exp} = 1, 2, 10, 20$ , and 500. Interesting enough,  $\kappa$  is basically independent on  $N_{exp}$ : the  $\kappa$  variation between  $N_{exp} = 1$  and 500 is lower than 2%. We also observe that  $\kappa$  is fully converged for any  $N_{exp} > 5$ . For this reason we choose  $N_{exp} = 5$  for the fitting procedure in all the AEMD simulations below.

### 3.5 $\kappa$ dependence on the fitting time interval

A key feature for the accuracy of the predicted value of  $\kappa$  is the extension of the time interval over which  $\Delta T(t)$  is fit. In other words, we could fit  $\Delta T(t)$  over the full time of simulation (Fig. 3) or for shorter intervals. We will refer to such time intervals as the fitting time  $t$ . Figure 6 shows the dependence of the calculated  $\kappa$  upon the fitting time in the range  $0$  ps  $\leq t \leq 200$  ps for a c-Si sample having a fixed length  $L_z = 162.91$  nm, section  $3.80 \times 3.80$  nm $^2$ , and  $\Delta T(0) = 200$  K. In this case  $\kappa$  strongly depends on  $t$ , in particular during the very first part of the simulation where the system is still far from the condition of thermal equilibrium and, therefore, long simulations seem necessary. In fact, a possible way to reduce the computational cost is to find a suitable fitting function able of reproducing the  $\kappa$  vs.  $t$  trend, so to extrapolate the fully converged thermal conductivity value  $\kappa_{conv}$  from a comparatively short simulation and, therefore, limiting the actual duration of the AEMD simulation. As shown in Figure 6, we have found a convenient function  $\kappa(t)$

$$\kappa(t) = \kappa_{conv} [1 - A \exp(-t/\tau)] \quad (18)$$

where  $\kappa_{conv}$ ,  $A$  and  $\tau$  are fitting parameters. The dashed line in Figure 6 represents the fitted  $\kappa(t)$  compared to the

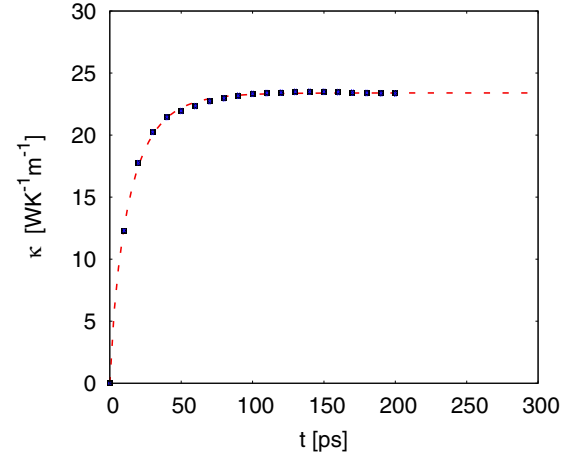


**Fig. 6.** Symbols: calculated  $\kappa$  vs. fitting time  $t$  for a c-Si sample with  $L_z = 162.91$  nm and  $S = 3.80 \times 3.80$  nm $^2$ . The dashed red line represents the fitting function  $\kappa(t) = \kappa_{conv}[1 - A \exp(-t/\tau)]$ .

actual  $\kappa$  directly obtained from the AEMD simulation. In order to quantify the error due to the present fitting procedure we compare the value of  $\kappa$  obtained by an AEMD run, as long as 200 ps with the corresponding  $\kappa_{conv}$  obtained from equation (18) where, however, a much shorter fitting time of 100 ps is used. The result is remarkable: using half the simulation time to fit  $\Delta T(t)$ , thus reducing remarkably the computational cost, the thermal conductivity was still estimated with an error smaller than 1%. This is the key feature of the present method which is greatly beneficial to minimize the overall computational cost and, therefore, to favor the application of AEMD to large system sizes.

### 3.6 $\kappa$ dependence on the sample length $L_z$

The study of the  $\kappa$  dependence on the sample length  $L_z$  represents an important issue for both NEMD and EMD calculations. In general, if  $L_z$  is shorter than the average phonon mean free path (MFP)  $\lambda$ , it is expected that  $\kappa = \kappa(L_z)$  since phonons having a mean free path  $\lambda > L_z$  will not contribute to the overall  $\kappa$  [8,24]. By increasing  $L_z$ , the probability that phonons are scattered before reaching the cell boundaries increases, giving rise to a diffusive regime (instead of ballistic-like transport).

As extensively discussed in reference [24], the  $\kappa$  dependence on  $L_z$  is explicitated as:

$$\kappa(L_z) = \frac{1}{N_q V} \sum_{q,s} c_{q,s} v_{q,s}^2 \tau_{\infty,q,s} \left[ 1 + \frac{2|v_{q,s}| \tau_{\infty,q,s}}{L_z} \right]^{-1} \quad (19)$$

where the sum takes into account all the phonon modes labeled by their momentum  $q$  and polarization  $s$ . The terms  $c_{q,s}$ ,  $v_{q,s}$  and  $\tau_{q,s}$  are, respectively, the heat capacity, the group velocity and the relaxation time for intrinsic phonon-phonon bulk-like scattering corresponding

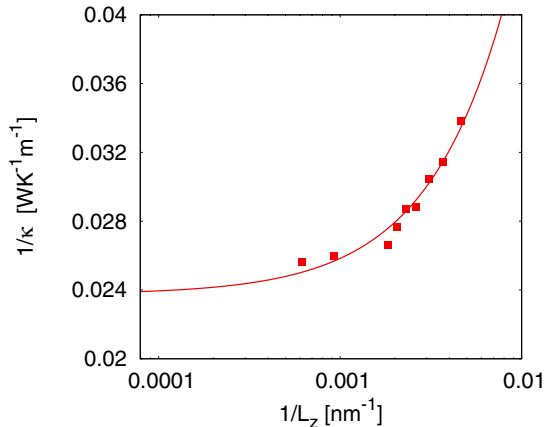


**Fig. 7.** Symbols:  $1/\kappa$  vs.  $1/L_z$  plot calculated by AEMD for a c-Si sample with  $S = 3.80 \times 3.80 \text{ nm}^2$  and  $108.61 \text{ nm} \leq L_z \leq 1629.15 \text{ nm}$ . Full line: linear fit (see text).

to each vibrational mode. According to equation (19) it is possible to write  $\frac{1}{\kappa} = f(\frac{1}{L_z})$ , i.e. it is possible to define a  $f$ -function converging to the inverse bulk value of thermal conductivity  $1/\kappa_\infty$  when  $L_z$  is large enough to mimic an infinite sample. Accordingly, it is possible to estimate  $\kappa_\infty$  by considering the Taylor expansion

$$\frac{1}{\kappa_\infty} = f(0) - \frac{f'(0)}{L_z} + \frac{f''(0)}{2L_z^2} + \dots \quad (20)$$

where apices indicate the order of derivation of the  $f$ -function. The resulting usual way of predicting  $\kappa_\infty$  in NEMD calculations consists in: (i) truncating equation (20) at the first order term and (ii) plotting  $1/\kappa$  versus  $1/L_z$  for a suitable range of sample lengths;  $\kappa_\infty$  is eventually obtained by extrapolating with a linear fit the NEMD data down to the  $1/L_z \rightarrow 0$  limit. This procedure is derived from the assumption that all the phonon modes in equation (19) have the same average properties. It has been shown in reference [24] that this assumption is not valid when the contribution to the thermal conductivity strongly depends on the single phonon modes. The only way to overcome this problem is to perform the above linear extrapolation procedure on simulation cells larger than (or, at least comparable to) the phonon MFP. By fully exploiting the reduced computational workload of AEMD, we can study  $\mu\text{m}$ -long simulation cells, thus meeting the above requirements for the reliability of the linear extrapolation procedure.

We investigate the  $\kappa$  dependence on the sample length  $L_z$  by simulating several periodically repeated cells with same section  $S = 3.80 \times 3.80 \text{ nm}^2$ , a  $\Delta T(0) = 200 \text{ K}$  and  $108.6 \text{ nm} \leq L_z \leq 1629.15 \text{ nm}$ . Figure 7 shows the corresponding  $1/\kappa$  vs.  $1/L_z$  plot. The extrapolated value of  $\kappa$  is equal to  $42 \pm 2 \text{ W m}^{-1} \text{ K}^{-1}$  to be compared with the experimental value [19]  $\kappa = 64 \text{ W m}^{-1} \text{ K}^{-1}$ . This result is very good, especially if contrasted with other calculations [20,21].

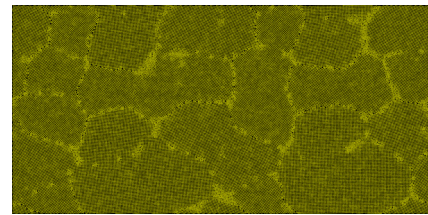


**Fig. 8.** Snapshot of the final configuration of a nc-Si sample with average grain size  $\langle d_g \rangle \sim 15 \text{ nm}$ . The sample has  $S = 2.715 \times 27.15 \text{ nm}^2$  and  $L_z = 81.5 \text{ nm}$ .

## 4 Benchmark applications

As commented above, one of the main advantages of the AEMD method is its computational cost with respect to other EMD and NEMD techniques. This reflects in the possibility to study very large systems, realistically reproducing the main structural features of experimental samples. Profiting of these advantages, here we focus on the study of thermal transport in nc-Si and a-Si: they are of great interest both for their intrinsic physical properties and for their possible use as energy materials. In addition, they can hardly be investigated with other MD methodologies affected by slow convergence, since they do require a combination of (very) large simulation cells and complex computer-generation procedures.

### 4.1 Nanocrystalline silicon

In this work nc-Si, is looked at as the prototypical example of a bulk nanostructured semiconductor with promising characteristics as highly efficient thermoelectric material [3,4]. The underlying physical idea is that by nanosstructuring conventional semiconducting materials it is possible to dramatically reduce the thermal conductivity without significantly affecting the corresponding electrical conductivity, thus increasing the overall figure of merit. This is due to the presence of internal boundaries (phase or grain boundaries) which maximize phonon scattering [3,4,25], therefore reducing the overall thermal conduction.

We generate atomistic models of nc-Si by following a multi-step procedure repeatedly applied to simulation cells that, by construction, have initially a cross section of  $2.715 \times 27.15 \text{ nm}^2$ .  $L_z$  was instead varied from  $81.5 \text{ nm}$  to  $190.10 \text{ nm}$  for the reasons discussed above. Each system was at first fully amorphized by quenching from the melt. Then, a number  $N_g$  of atom sites were selected at random in the  $yz$  plane and around each of them a cylindrical void was created by removing atoms. Voids were distributed avoiding overlap; also their initial radius was randomly set above the capillarity threshold ( $\sim 0.5 \text{ nm}$ ) [26]. Next, each void was filled by a crystalline seed randomly rotated in the  $yz$  plane. The resulting mixed structures were annealed at constant  $T = 1200 \text{ K}$  for times up to  $4.0 \text{ ns}$ . During annealing the seed grains underwent growth through solid state epitaxy, until full recrystallization occurred. Figure 8 shows a snapshot of the final configuration for

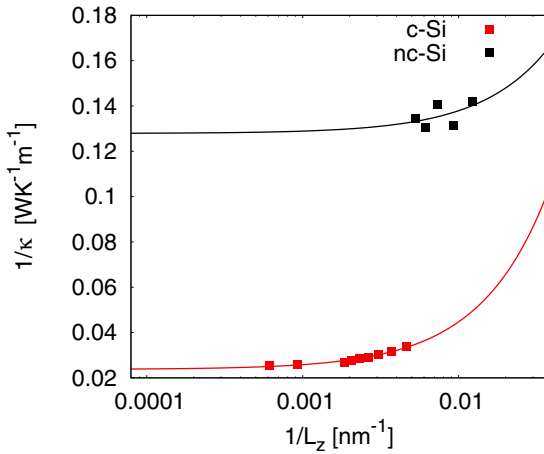


**Fig. 9.** Black symbols:  $1/\kappa$  vs.  $1/L_z$  plot calculated by AEMD for nc-Si samples with  $81.5 \text{ nm} \leq L_z \leq 190.10 \text{ nm}$ . Red Symbols :  $1/\kappa$  vs.  $1/L_z$  plot calculated by AEMD for c-Si samples with  $108.61 \text{ nm} \leq L_z \leq 1629.15 \text{ nm}$ . Full lines: linear fit (see text).

a nc-Si sample having cross section of  $2.715 \times 27.15 \text{ nm}^2$  and  $L_z = 81.5 \text{ nm}$ . In total we generated a set of ten different templates, with average grain size  $\langle d_g \rangle \sim 15 \text{ nm}$ . The values of thermal conductivity discussed below were obtained as the  $1/L_z \rightarrow 0$  extrapolation of a set of  $\kappa$  values corresponding to such samples.

Figure 9 shows the  $1/\kappa$  vs.  $1/L_z$  plot (black curve) for nc-Si together with the case of crystalline Si (red curve), both calculated at  $T = 600 \text{ K}$  with  $\Delta T(0) = 200 \text{ K}$ . It is quite evident the main effect of grain boundaries to reduce the thermal conductivity by increased phonon scattering:  $\kappa$  in nc-Si is estimated to be, as low as  $7.8 \pm 0.1 \text{ W m}^{-1} \text{ K}^{-1}$ , in contrast to the  $42 \pm 1 \text{ W m}^{-1} \text{ K}^{-1}$  value calculated for a c-Si sample with same dimensions. This conclusion is confirmed by the calculation of thermal conductivity accumulation function (TCAF), here defined as the ratio  $\kappa(L_z)/\kappa_\infty$  between its value computed for a simulation cell with length  $L_z$  and its corresponding extrapolated value for a bulk-like (infinite) sample.  $\kappa(L_z)/\kappa_\infty$  gives the contribution to the thermal conductivity provided by phonons with mean free path (MFP) up to  $L_z$ . In Figure 10 it is shown that for a nc-Si sample as much as  $\sim 90\%$  of the thermal conductivity is provided by vibrational modes with  $\text{MFP} \leq 100 \text{ nm}$ . On the other hand, for c-Si the same contribution is provided by phonons with  $\text{MFP} \leq 1 \mu\text{m}$  [24]. Therefore, we conclude that the reduction of thermal conductivity of nc-Si predicted by the present AEMD analysis is mainly due to the grain boundary scattering of phonons with long MFP.

## 4.2 Amorphous Si

We next move to the investigation of thermal transport in a-Si, which is still a matter of discussion in recent literature [7,27–29]. Thermal conductivity in this material is sometimes described by means of diffusons, i.e. non-propagating localized vibrational modes. Recently, how-

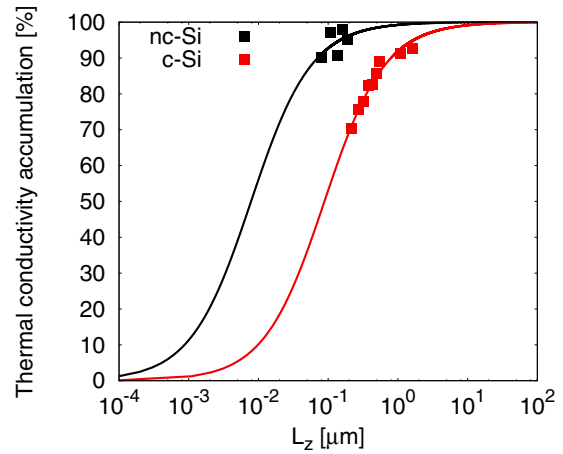


**Fig. 10.** Symbols: thermal conductivity accumulation function calculated by AEMD for nc-Si (black) and c-Si (red). Full lines: corresponding accumulation function obtained by the linear fit (see text).

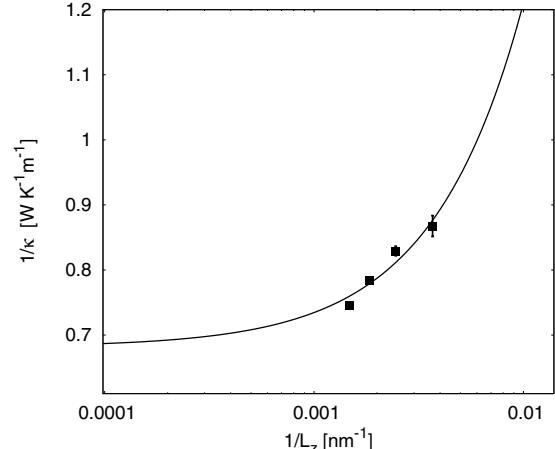


**Fig. 11.**  $1/\kappa$  vs.  $1/L_z$  plot obtained by AEMD for a-Si samples with  $S = 3.80 \times 3.80 \text{ nm}^2$  and  $271.5 \text{ nm} \leq L_z \leq 678.8 \text{ nm}$ . Full line: linear fit (see text).

ever, it has been shown that thermal conductivity in a-Si is also due to phonon-like diffusive modes, having mean free paths longer than  $100 \text{ nm}$ , which provide a sizeable contribution [7,27]. Here, we investigate the issue whether thermal conduction is diffuson-dominated or phonon-dominated, taking full profit of AEMD which easily allows to access cell dimensions comparable to the maximum vibrational mean free paths in a-Si.

We generate amorphous samples by quenching from the melt [26] several samples with  $S = 3.80 \times 3.80 \text{ nm}^2$  and  $271.5 \text{ nm} \leq L_z \leq 678.8 \text{ nm}$ . In Figure 11 it is shown the usual  $1/\kappa$  vs.  $1/L_z$  plot. The corresponding extrapolated  $\kappa$  value is  $1.5 \pm 0.02 \text{ W m}^{-1} \text{ K}^{-1}$  which is actually in very good agreement with the recent experimental value  $1.7 \text{ W m}^{-1} \text{ K}^{-1}$  reported in reference [7].

A deeper analysis of a-Si thermal conductivity is obtained by calculating the TCAF. Also, we want to compare the TCAF at  $300 \text{ K}$  of a-Si with its crystalline counterpart, i.e. with a material with same chemistry but a definitely

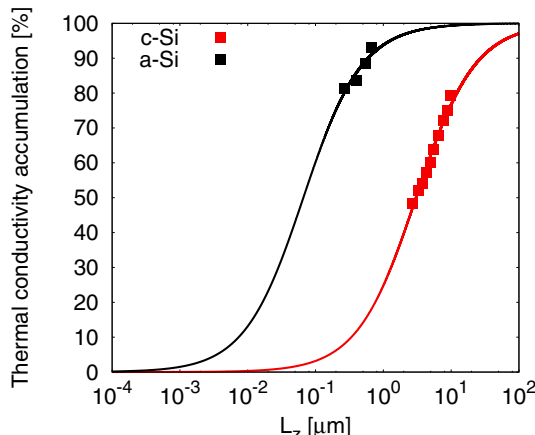


**Fig. 12.** Symbols: thermal conductivity accumulation function calculated by AEMD for c-Si (red) and a-Si (black). Full lines: corresponding accumulation function obtained by the linear fit (see text).

phonon-dominated thermal conductivity. In order to calculate the TCAF of c-Si at 300 K we have to consider simulations cells having  $L_z$  in the order of several  $\mu\text{m}$ . The use of such a large simulation cells is demanded by the fact that recent experiments pointed out that 40% of the total thermal conduction of c-Si at 300 K is due to phonons having MFP longer than 1  $\mu\text{m}$  [7,28,29]. For this reason we consider simulation cells with  $2715.2 \text{ nm} \leq L_z \leq 9777.5 \text{ nm}$ . We emphasize that such dimensions are, to the best of our knowledge, unprecedented in any EMD or NEMD calculations.

Figure 12 shows the TCAF calculation for a-Si and c-Si. In the case of a-Si as much as  $\sim 50\%$  of  $\kappa$  is due to diffuson-like modes having  $\lambda < 100 \text{ nm}$ , while the remaining contribution is due to diffusive phonon-like modes with  $\lambda > 100 \text{ nm}$ . This result is in agreement with recent EMD calculations showing basically the same trend [27]. On the other hand, Figure 12 shows that in c-Si most of  $\kappa$  is actually due to phonons having much longer MFP with respect to a-Si. In particular, we conclude that  $\sim 50\%$  of  $\kappa$  is due to phonons with  $\lambda > 1 \mu\text{m}$ , in very good agreement with the recent experimental results of reference [7].

## 5 Conclusions

We have assessed basics, accuracy, and performances of a nonequilibrium MD method (referred to as AEMD) for the calculation of lattice thermal conductivity in a transient regime of approach to equilibrium. We have shown that AEMD is theoretically robust and numerically accurate, since the calculated  $\kappa$  values are basically independent of most arbitrary simulation parameters. In addition, we have provided evidence that AEMD is characterized by ease of implementation and low computational workload. This allows for the investigation of realistically complex systems. In this paper, we focused on the description of lattice thermal transport in nc-Si and a-Si systems, here presented of paradigmatic examples of semiconductor

materials with large potential impact as energy materials. The results for  $\kappa$  show a good agreement with recent experimental measurements, as well as with other theoretical calculations. They also provide a clean picture on the role of grain boundaries and lattice disorder to affect the contribution to thermal conductivity of vibrational modes with long mean free paths.

We acknowledge useful discussions with E. Lampin, P.L. Palla and F. Cleri (University of Lille), financial support under project PRIN-GRAF funded by MIUR and computational support by ISCRA-CINECA Project THEBUNA. We also acknowledge K. Hahn (University of Cagliari) for a critical reading of this manuscript.

## References

1. T.L. Bergman, A.S. Lavine, F.P. Incropera, D.P. DeWitt, *Fundamentals of Heat and Mass Transfer* (John Wiley & Sons, USA, 2002)
2. J.H. Lienhard IV, J.H. Lienhard V, *A heat transfer textbook* (Phlogiston Press, Cambridge, 2006)
3. M.S. Dresselhaus, G. Chen, M.Y. Tang, R. Yang, H. Lee, D. Wang, Z. Ren, J.-P. Fleurial, *Adv. Mater.* **19**, 1043 (2007)
4. A.J. Minnich, M.S. Dresselhaus, Z.F. Ren, G. Chen, *Energy Environ. Sci.* **2**, 466 (2009)
5. G.J. Snyder, E.S. Toberer, *Nat. Mater.* **7**, 105 (2008)
6. G.S. Nolas, J. Sharp, H. Goldsmid, *Thermoelectrics: Basic Principles and New Materials Developments* (Springer, New York, 2001)
7. K.T. Regner, D.P. Sellan, Z. Su, C.H. Amon, A.J.H. McGaughey, J.A. Malen, *Nat. Commun.* **4**, 1640 (2013)
8. P.K. Schelling, S.R. Phillpot, P. Kebinski, *Phys. Rev. B* **65**, 144306 (2002)
9. Y. He, I. Savić, D. Donadio, G. Galli, *Phys. Chem. Chem. Phys.* **14**, 16209 (2012)
10. J. Garg, N. Bonini, B. Kozinsky, N. Marzari, *Phys. Rev. Lett.* **106**, 045901 (2011)
11. J.-S. Wang, J. Wang, J.T. Lu, *Eur. Phys. J. B* **62**, 381 (2008)
12. E. Lampin, P.L. Palla, P.-A. Franciosi, F. Cleri, *J. Appl. Phys.* **114**, 033525 (2013)
13. E. Lampin, Q.-H. Nguyen, P.A. Franciosi, F. Cleri, *Appl. Phys. Lett.* **100**, 131906 (2012)
14. C. Melis, L. Colombo, *Phys. Rev. Lett.* **112**, 065901 (2014)
15. D.A. McQuarrie, *Statistical Mechanics* (University Science Books, Sausalito, 2000)
16. F. Müller-Plate, *J. Chem. Phys.* **106**, 6082 (1997)
17. A.J.H. McGaughey, C.H. Amon, J.E. Turney, E.S. Landry, *Phys. Rev. B* **79**, 064301 (2009)
18. N.W. Ashcroft, N.D. Mermin, *Solid State Physics* (Holt-Sanders International Editions, London, 1976)
19. C.J. Glassbrenner, G.A. Slack, *Phys. Rev.* **137**, A1058 (1964)
20. C. Abs da Cruz, K. Termentzidis, P. Chantrenne, X. Kleber, *J. Appl. Phys.* **110**, 034309 (2011)
21. P.C. Howell, *J. Chem. Phys.* **137**, 224111 (2012)

22. S. Plimpton, J. Comput. Phys. **117**, 1 (1995). See also the following site: <http://lammps.sandia.gov>
23. J.F. Justo, M.Z. Bazant, E. Kaxiras, V.V. Bulatov, S. Yip, Phys. Rev. B **58**, 2539 (1998)
24. D.P. Sellan, E.S. Landry, J.E. Turney, A.J.H. McGaughey, C.H. Amon, Phys. Rev. B **81**, 214305 (2010)
25. W. Jang, J.E. Garay, C. Dames, Z. Wang, J.E. Alaniz, Nano Lett. **6**, 2206 (2011)
26. A. Mattoni, L. Colombo, Phys. Rev. B **78**, 075408 (2008)
27. Y. He, D. Donadio, G. Galli, Appl. Phys. Lett. **98**, 144101 (2011)
28. J. Cue, J.K. Eliason, A.J. Minnich, T. Kehoe, C.M.S. Torres, G. Chen, K.A. Nelson, J.A. Johnson, A.A. Maznev, Phys. Rev. Lett. **110**, 1079 (2010)
29. G. Chen A.S. Henry, J. Comput. Theor. Nanosci. **5**, 1 (2013)